(4)

OFFICE OF NAVAL RESEARCH

Contract N00014-87-J-1118

R & T Code 4133016

Technical Report No. 10

Evidence for a Photon-Driven Charge-Transfer Enhancement in the Surface-Enhanced Raman Scattering of DABCO at a Silver Electrode

by

D.A. Guzonas, D.E. Irish and G.F. Atkinson

Prepared for Publication

in

Langmuir

Guelph-Waterloo Center for Graduate Work in Chemistry
Waterloo Campus
Department of Chemistry
University of Waterloo
Waterloo, Ontario
Canada, N2L 3G1

August 9, 1989

SECURITY CLASSIFICATION OF THIS PAGE

REPORT DOCUMENTATION PAGE

1a REPORT SECURITY CLASSIFICATION Unclassified	1b RESTRICTIVE MARKINGS
2a SECURITY CLASSIFICATION AUTHORITY Unclassified	3 DISTRIBUTION / AVAILABILITY OF REPORT Public Release/Unlimited
2b DECLASSIFICATION / DOWNGRADING SCHEDULE	
4 PERFORMING ORGANIZATION REPORT NUMBER(S) ONR Technical Report #10	5 MONITORING ORGANIZATION REPORT NUMBER(S)
6a NAME OF PERFORMING ORGANIZATION D. E. Irish University of Waterloo 6b OFFICE SYMBOL (If applicable)	7a NAME OF MONITORING ORGANIZATION Office of Naval Research
6c ADDRESS (City, State, and ZIP Code) Department of Chemistry University of Waterloo Waterloo, Ontario, Canada N2L 3G1	7b ADDRESS (City, State, and ZIP Code) The Ohio State University Research Center 1314 Kinnear Road, Room 318 Columbus, Ohio, U.S.A. 43212-1194
8a NAME OF FUNDING/SPONSORING ORGANIZATION Office of Naval Research 8b OFFICE SYMBOL (If applicable)	9 PROCUREMENT INSTRUMENT IDENTIFICATION NUMBER N00014-87-J-1118
8c ADDRESS (City, State, and ZIP Code) Chemistry Division 800 N Quincy Street Arlington, VA, U.S.A., 22217-5000	10 SOURCE OF FUNDING NUMBERS PROGRAM ELEMENT NO / PROJECT NO / TASK NO / WORK UNIT ACCESSION NO

11 TITLE (Include Security Classification)
Evidence for a Photon-Driven Charge-Transfer Enhancement in the Surface Enhanced Raman Scattering of DABCO at a Silver Electrode

12 PERSONAL AUTHOR(S)
David A. Guzonas, Donald E. Irish* and George F. Atkinson

13a TYPE OF REPORT	13b TIME COVERED FROM 08/88 TO 08/89	14 DATE OF REPORT (Year, Month, Day)	15 PAGE COUNT
		1989-8-9	51

16 SUPPLEMENTARY NOTATION
Prepared for Langmuir

17 COSATI CODES			18 SUBJECT TERMS (Continue on reverse if necessary and identify by block number)
FIELD	GROUP	SUB-GROUP	
			SERS Mechanism; Raman; DABCO

19 ABSTRACT (Continue on reverse if necessary and identify by block number)

The surface-enhanced Raman (SER) spectra of the alphatic amine 1,4-diazabicyclo(2.2.2)octane adsorbed on the surface of silver electrodes has been studied in detail as a function of the electrode potential and the excitation energy. Variations in the SERS intensity resulting from the variation in these two parameters and the supporting electrolyte have been characterized and attributed to the existence of a photon-driven charge-transfer (PDCT) enhancement of one to two orders of magnitude, of the adsorbed DABCO molecule, which operates in addition to an electromagnetic enhancement. The direction of the charge transfer is from molecule to metal. Variations in the band frequencies of the adsorbed DABCO with electrode potential and with the supporting electrolyte have also been measured and ascribed to the existence of a ground state charge transfer between adsorbed DABCO and the silver electrode. The Raman spectrum of a charge-transfer complex between DABCO and iodine are presented for comparison. (KR)

20 DISTRIBUTION / AVAILABILITY OF ABSTRACT	21 ABSTRACT SECURITY CLASSIFICATION
☒ UNCLASSIFIED/UNLIMITED ☐ SAME AS RPT ☐ DTIC USERS	Unclassified
22a NAME OF RESPONSIBLE INDIVIDUAL Dr. Robert J. Nowak	22b TELEPHONE (Include Area Code) (519) 885-1211 ext. 2500
	22c OFFICE SYMBOL

DD FORM 1473, 84 MAR 83 APR edition may be used until exhausted
All other editions are obsolete

SECURITY CLASSIFICATION OF THIS PAGE
Unclassified

Evidence For a Photon-Driven Charge-Transfer Enhancement in The Surface Enhanced Raman Scattering of DABCO at a Silver Electrode.

David A. Guzonas
Donald E. Irish *
George F. Atkinson

Guelph-Waterloo Center for Graduate Work in Chemistry
Waterloo Campus, Department of Chemistry, University of Waterloo,
Waterloo, Ontario N2L 3G1
Canada

ABSTRACT

The surface-enhanced Raman (SER) spectra of the aliphatic amine 1,4- diazabicyclo[2.2.2]octane adsorbed on the surface of silver electrodes has been studied in detail as a function of the electrode potential and the excitation energy. Variations in the SERS intensity resulting from the variation in these two parameters and the supporting electrolyte have been characterized and attributed to the existence of a photon-driven charge-transfer (PDCT) enhancement of one to two orders of magnitude, of the adsorbed DABCO molecule, which operates in addition to an electromagnetic enhancement. The direction of the charge transfer is from molecule to metal. Variations in the band frequencies of the adsorbed DABCO with electrode potential and with the supporting electrolyte have also been measured and ascribed to the existence of a ground state charge transfer between adsorbed DABCO and the silver electrode. The Raman spectrum of a charge-transfer complex between DABCO and iodine are presented for comparison.

Introduction

The application of surface enhanced Raman scattering (SERS) to the study of electrochemical systems is still hindered by a lack of understanding of the role played by possible "chemical" enhancement mechanisms. Although the contribution to the overall

enhancement of the electromagnetic (EM) enhancement mechanism is fairly well understood, controversy still exists over the degree to which other mechanisms such as those involving charge-transfer contribute to the total enhancement (For recent reviews see Ref. 1 and 2). One such 'chemical' mechanism is the photon-driven charge-transfer (PDCT) mechanism which originated in a verbal description by Burstein et al. (3) of a number of mechanisms for coupling electron-hole pair excitations in the metal to molecular vibrations. A more explicit treatment was given by Gersten et al.(4); similar ideas have been proposed by other authors (5,6,7,8,9). In a recent paper (10), we have proposed that the SERS of the diamine DABCO (1,4- diazabicyclo[2.2.2.]octane) involves a contribution from such a photon-driven charge-transfer mechanism.

A simplified description of the proposed model follows. Figure 1 illustrates the model system of an adsorbed DABCO molecule at a metal surface. The highest occupied molecular orbital (HOMO) of DABCO is represented by $|a>$ of energy ϵ_a and the lowest unoccupied molecular orbital (LUMO) is represented by $|b>$ of energy ϵ_b. The essence of the PDCT model is that the continuum of metal states can act as intermediate states in a resonance Raman-like process, such as that shown in Figure 1. Here, an electron-hole (e-h) pair is produced in the metal by the incident photon; the hole tunnels to the HOMO of DABCO, where it may reside briefly before tunneling back to the metal to recombine with the electron and emit a photon. If during the residence time of the hole on the molecule the molecule relaxes to a new equilibrium geometry, the hole may lose energy, and upon recombination a Raman-shifted photon will be emitted. This model equivalently involves a charge-transfer from the HOMO of adsorbed DABCO to the metal. On the basis of earlier work by Heilbronner and Muszkat (11) on the photoelectron spectroscopy of DABCO, such a charge-transfer process is expected to preferentially excite four of the totally symme-

tric modes of DABCO. Such a selective enhancement is indeed observed (10). To provide further evidence for the existence of a PDCT enhancement of DABCO adsorbed on a silver surface, we have made a detailed study of the dependence of the SERS intensities and frequencies on the electrode potential and the excitation wavelength.

We have also prepared a DABCOI_2 charge transfer complex (12) and measured its Raman spectrum for comparison to that of the SER spectra.

Experimental

The electrochemical cells, potentiostat, and computer interfaced Jarrell-Ash scanning spectrometer have been described in a previous paper (10). A DILOR OMARS 89 spectrometer with optical multichannel detection (OMA), interfaced to an Apple IIe computer, was also used. Laser excitation was provided by a Spectra-Physics 165-08 Argon ion laser (lines at 514.5, 501.7, 495.6, 476.5, and 457.9 nm were used) or by a Coherent Krypton ion laser (lines at 568.2, 647.1 and 676.4 nm).

DABCO, 97% (Aldrich Chemical Co.) was purified by recrystallization from 60-80 degree b.p. pet ether or sublimed under reduced pressure. KCl, KBr, NaF, $NaClO_4$ were all reagent grade. Distilled, deionized water was used for preparation of solutions; all solutions were purged with nitrogen gas for one hour prior to the SERS experiments.

The DABCO-iodine charge transfer complex was prepared according to the method of Halpern and Weiss (12). 91.4 mg of iodine in 25 ml of n-heptane were mixed with 25 ml of n-heptane containing 41 mg of sublimed DABCO. Immediately a reddish-orange fine precipitate formed, which was dried and stored in a desiccator until used.

As in (10), the measurement of the potential profiles was performed using the method of Billmann and Otto (13) and Furtak and Macomber (14). By opening the spectrometer slits to a bandpass of 15 cm^{-1}, setting the monochromator at the center of the SERS band of interest and sweeping the electrode potential while recording the SERS intensity on a strip chart recorder, a plot of the variation of the integrated band area versus the electrode potential was obtained. Wide slits were required because the SERS bands shift in frequency as a function of the electrode potential; even with this wide slitwidth, considerable care was needed in order to obtain meaningful potential profiles at higher photon energies because of the sometimes substantial (up to 14 cm^{-1}) band shifts in going from -100 to -1000 mV.

A dependence of the intensity on the laser power was observed, this effect being quite pronounced in that changing the laser power by one order of magnitude, from 200 mW to 20 mW, shifts the potential at which the SERS intensity maximizes by 120 mV in the cathodic direction. This may be evidence for a photochemical degradation of DABCO or perhaps the effect of laser heating. It was found that this laser power dependence was minimal or absent for laser powers of 20 mW or less, and thus all potential profile measurements were performed using laser powers in this range.

The experimental procedure for the measurement of the potential profiles was to first polish the electrode, introduce it into the cell under potential control, roughen the electrode and, after a fixed time interval, sweep the electrode potential in a cathodic direction. At the cathodic limit the potential would be either removed and the electrode removed from the cell, or stepped back to the starting potential and a second (and possibly third) cathodic sweep performed. After removing the electrode from the cell, it was repolished and then the entire experiment repeated at least once more at the same excitation wavelength. The potential profiles were obtained for at least five excitation wavelengths if possible. The potential sweep started at an anodic

limit determined by the supporting electrolyte used, and a cathodic limit of -1000 mV or more cathodic, with a sweep rate of 5 mV/s.

The excitation profile experiments were performed by roughening the electrode in-situ and then potentiostating the electrode at a chosen potential. The spectral region of interest was scanned and the exciting line was then changed, an effort being made to be sure that the same spot on the electrode was always being illuminated by the beam. Once a set of spectra was obtained, the spectra were baseline corrected and the SERS bands of interest as well as the unenhanced Raman spectrum of the standard were integrated, either by computer or by planimeter. When severe band overlap was present, the spectra were curve resolved using a modified BNDFT programs (15).

Results and Discussion

Figure 2 shows the SER spectrum of DABCO adsorbed on a silver electrode at a potential of -500 mV, excited using 568.2 nm excitation, and a normal Raman spectrum of a 2 M aqueous solution of DABCO excited by 700 mW of the 514.5 nm argon ion laser line. Figure 3 shows the Raman spectrum of the charge-transfer complex DABCO-I_2, excited using 20 mW of 568.2 nm excitation, obtained using the microscope accessory of the DILOR OMARS-89. It is clear that both the SER spectrum and the spectrum of the charge-transfer complex are substantially very similar, in that only four bands appear with large intensity in the spectral region from 300-1600 cm^{-1}, and that the Raman bands in both spectra exhibit radically altered relative intensities compared to the solution Raman spectrum. The four bands which dominate the SER spectrum and the spectrum of the charge-transfer complex are ν_3 ($w\,CH_2$ / νCC), found at 1352 cm^{-1} in solution, 1351 cm^{-1} in the SER spectrum and 1353 cm^{-1} in the C-T complex, ν_4 (νCC/ wCH_2) found at 983 cm^{-1} in solution, 986 cm^{-1} in the SER spectrum and 993 cm^{-1} in the C-T complex, ν_5 ($\nu_s NC_3$), found

at 806 cm^{-1} in solution, 794 cm^{-1} in the SER spectrum and 798 cm^{-1} in the C-T complex, and ν_6 (*skeldef*), found at 630 cm^{-1} in solution, 617 cm^{-1} in the SER spectrum and 643 cm^{-1} in the spectrum of the C-T complex. Recently, Santos and Mello (16) have published the Raman spectra of molecular complexes of DABCO with iodine, bromine, sulfur dioxide, carbon tetrabromide, iodoform and phenol; in those spectra selective enhancement of ν_3, ν_4, ν_5 *and* ν_6 was observed. The strength of the intensity enhancement correlates with the polarizability of the acceptor molecule. The band assignments are from reference 17. The close similarity between the SER spectrum and the spectrum of the C-T complex suggests that they arise from a similar process, namely a charge-transfer excitation involving the DABCO molecule as an electron donor. We believe that, in the SERS experiments, the charge-transfer excitation gives rise to an enhancement of one to two orders of magnitude, on top of an electromagnetic enhancement of up to four orders of magnitude. Further evidence for this hypothesis will be given below.

An empirical equation for the SERS intensity I_j^i of a vibrational band of frequency ω_i of a species j, in the presence of species k (e.g., supporting electrolyte), excited using a laser of frequency ω_L can be written as:

$$I_j^i(U, \omega_L, \omega_i, C_j, C_k) \propto \theta(U, C_j, C_k) \cdot F_{EM}^i(\omega_L, \omega_i) \cdot F_{PDCT}^i(U, \omega_L, \omega_i) \cdot |\vec{E}|^2$$

Here, U is the electrode potential, θ_j is the surface coverage, F_{EM} is the electromagnetic enhancement factor, F_{PDCT} is the enhancement due to the PDCT mechanism, C_j and C_k are the bulk concentrations of the jth and kth species, and $\vec{E}$ is the electric field vector of the incident laser radiation. If the SERS experiment is carried out at constant solution composition, then equation 1 can be rewritten as

$$I_j^i(U, \omega_L, \omega_i) \propto \theta_j(U) \cdot F_{EM}(\omega_L, \omega_i) \cdot F_{PDCT}(U, \omega_L, \omega_i) \cdot |\vec{E}|^2$$

. There are thus two kinds of experiment which can be performed in an electrochemical SERS system in order to probe the relative importance of the two mechanisms. Experiments carried out at constant wavelength in which the dependence of the intensity on the electrode potential is measured will be referred to as potential profiles, while experiments performed at constant electrode potential in which the dependence of the intensity on the excitation wavelength is measured will be denoted as excitation profiles. The SERS intensities of the band ω_i for these two types of measurements are given by

$$(I_j^i(U))_{\omega_L} \propto \theta_j(U) \cdot (F_{EM})_{\omega_L} \cdot (F_{PDCT}(U))_{\omega_L} \cdot |\vec{E}|^2$$

and

$$(I_j^i(\omega_L))_U \propto (\theta_j)_U \cdot F_{EM}(\omega_L) \cdot (F_{PDCT}(\omega_L))_U \cdot |\vec{E}|^2$$

where the subscripts denote the variable held constant, and $(F_{EM})_{\omega_L}$ and $(\theta_j)_U$ are assumed to be simple numerical constants at the chosen values of the superscripts. It is clear from the forms of these expressions that neither one of these measurements of intensity will yield unambiguous information concerning the role played by F_{EM} or F_{PDCT}, since both intensity profiles are the product of two enhancement factors. However, the coverage term is not dependent upon the excitation wavelength, so that measurements of the potential profiles at several excitation wavelengths will reveal any contribution to these profiles of the PDCT mechanism. In a similar manner, the measurement of the excitation profiles at several values of the electrode potential will aid in the identification of contributions to these curves from the potential dependent F_{PDCT} term.

Potential Profiles

The PDCT model makes a very specific prediction about the variation of the SERS intensity with the electrode potential. The existence of a resonance condition

$$\epsilon - \epsilon_a = 0$$

where ϵ is the photon energy and ϵ_a is the energy of the molecular level $|a>$, measured with respect to the Fermi level, implies that the SERS intensity will pass through a maximum when this condition is met. This expression can be recast into terms which are measured in an electrochemical experiment:

$$\hbar\omega_L = U_o - U_m$$

where U_m is the electrode potential at which the maximum SERS intensity is observed, U_o is the reference potential and $\hbar\omega_L$ is the laser energy in eV. The reference potential chosen for the measurement of U_m is that potential at which the DABCO HOMO and the Fermi level are aligned, i.e., the oxidation potential of DABCO, measured with respect to the reference electrode in use, in the present case the SCE. One indeed finds that there is a marked dependence of the potential at which this maximum occurs on the excitation wavelength; however, difficulties arise when one attempts to quantify these observations. The SERS bands were scanned rapidly at several electrode potentials, and representative spectra are illustrated in Figure 4 for ν_4 at three excitation wavelengths. There is an obvious shift in the potential at which the intensity of the band in this figure maximizes as the excitation wavelength is altered. Because of concern over the long time period during which the electrode was illuminated by the laser, the potential profiles were not measured by measuring discrete spectra, but by the potential sweep method described in the experimental section. A check on the reproducibility showed that the potential of the maximum inte , could be reproduced to within 50 mV at low photon energy

(Krypton laser lines) but the reproducibility became worse as the photon energy increased . It was observed that the background intensity also varied with the electrode potential but that this variation was much less than that of the SERS band, and that interestingly, the two maximize at about the same electrode potential, suggesting a common origin for the intensity variation. The effect of multiple cycles was explored using electrodes which were scanned to very cathodic potentials and then remeasured without reroughening of the electrode. Although the intensity variation was often found to decrease with increasing number of sweeps, the position of the maximum did not vary by more than 30 mV, suggesting that the position of the maximum is independent of any surface changes which may occur during the cathodic sweep. The irreversible loss of adatoms may be one surface process causing a loss of intensity, but it must be pointed out that this loss of intensity was not always observed and may arise from the presence in the system of surface contaminants which poison the surface during the first cathodic sweep. However, the fact that the position of the maximum is independent of the number of sweeps is sufficient to confirm the validity of this method of potential profile measurement.

Potential profiles of ν_4 of DABCO at a silver electrode in 0.1 M $KClO_4$, 0.05 M DABCO recorded at different excitation wavelengths are illustrated in Figure 5. In accord with the prediction of the PDCT model proposed for DABCO, the potential at which the SERS intensity maximizes shifts to more negative values as the photon energy is increased (shorter wavelength). This behavior also illustrates that the observed intensity changes in the SER spectra of DABCO with changes in the electrode potential are not related to the coverage in a simple manner, since the position of the maximum in the intensity is wavelength dependent. The existence of coverage effects may account for another phenomenon which is observed in these curves, viz., the decrease in the overall intensity of the curves, as witnessed by the lower S/N

ratio for the potential profile measured using 488.0 nm excitation, as the excitation wavelength is made shorter. Since the curves at shorter wavelength excitation are also measured at more negative electrode potential, this could be evidence that the coverage of DABCO is reduced at more cathodic potentials, resulting in a reduced overall intensity in the potential profiles. An alternate explanation for this observation is that the SERS enhancement is greater at longer wavelength excitation because of the SERS mechanism; this will be discussed in the section on SERS excitation profiles.

The magnitude of the intensity changes observed in the potential profiles gives an indication of the size of the enhancement arising from the PDCT enhancement mechanism. For example, the potential profile measured at 647.1 nm in Figure 5 decreases in intensity by about one order of magnitude between its maximum intensity at about -100 mV and its minimum intensity at -1100 mV. In all potential profiles measured the difference in intensity between maximum and minimum was between one to two orders of magnitude, suggesting that the PDCT contribution to the total surface enhancement for DABCO is one to two orders of magnitude.

Since the supporting electrolyte plays a role in the adsorption behavior of DABCO, it was of interest to see what effect, if any, the supporting electrolyte would have on the shape and positions of the potential profiles. That such an effect exists has been demonstrated for pyridine by Furtak and Macomber (14) and by Billmann and Otto (13) Potential profiles were measured for DABCO in the presence of the anions Cl^-, Br^- and ClO_4^-, the latter two being only weakly specifically adsorbed anions. Distinct differences in the potential profiles for DABCO in the presence of these three anions are observed , and these differences are more pronounced for the potential profiles obtained with longer wavelength excitation than at shorter wavelength excitation. This can be clearly seen in Figure 6, where the potential profiles for 676.4 nm excitation are shown for all three electrolytes. The shift of the potential

profiles is toward more anodic potentials in the order $ClO_4^- > F^- > Cl^-$.

As first noted by Jeanmaire and Van Duyne (18) during their pioneering work on SERS, the potential profiles of different bands in the SER spectrum of an adsorbate (in their case pyridine) do not maximize at the same electrode potential. This observation has been reported by a number of other groups with respect to a wide variety of adsorbates but has not yet been adequately explained. The values of U_m at six excitation wavelengths in 0.1 M KCl are given in Table I for each of the four strongest DABCO modes, and a plot of U_m versus the photon energy for these four modes is presented in Figure 7. The data were fit using a linear least squares routine and the slope and intercept are also listed in Table I; the lines through the data points for ν_3, ν_5, and ν_6 are seen to be nearly parallel, but offset from all of the others; the slope for ν_4 is slightly different. There appears to be no pattern to the offset, and the data for ν_3 and ν_4 do not coincide even though both modes contain the same two symmetry co-ordinates. This non-coincidence of the potential profiles of the DABCO a_1' modes is very similar to the behavior of the pyridine totally symmetric modes reported by Thietke et al., (19). Similarly , the potential profiles measured in fluoride and perchlorate supporting electrolytes for different modes do not maximize at the same electrode potential. The values of U_m for the perchlorate and fluoride electrolytes are listed in Table II; the data for ν_4, for all three supporting electrolytes are plotted in Figure 8. The slope and intercept of the best fit straight line to the data are also listed in Table II; the theoretically expected value of negative one is found only for the perchlorate supporting electrolyte.

How does the specific adsorption of chloride change the behavior of the potential profiles? Consider the case of no specific adsorption, the electrode being held at a potential U_o. At this potential the electrode has a charge σ_m^o. The addition of specifi-

cally adsorbable anions to the solution will result in the specific adsorption of some of these anions, the extent of the adsorption (surface excess) depending upon the bulk anion concentration. This specific adsorption of negative charges at the surface induces a positive countercharge in the highly polarizable electrode, the new electrode charge being σ_m'. Thus, at a constant applied potential U_o, the electrode charge σ_m' will be more positive, $\sigma_m' > \sigma_m^o$, in the presence of the specifically adsorbed anions. In order to obtain the same electrode charge σ_m^o, the applied potential will have to be made more negative, to U. This argument explains the shift of the point of zero charge (pzc) to more cathodic potentials with specific adsorption, and also can explain the shift in potential profiles. Furtak and Macomber (14) have shown that the shift is also dependent upon the concentration of the anion in a manner consistent with the above argument.

This explains the shift in the position of U_{max} in the presence of chloride, but what is the origin of the large difference in slopes for the data obtained in perchlorate and fluoride solutions, since both of these anions are only slightly specifically adsorbed on silver? One would have expected *a priori* that the slopes of the two lines for these anions would have been very similar, if not identical, but as Figure 8 shows, the variation in slope between fluoride and perchlorate is actually greater than that between fluoride and chloride. The deviation of the observed slope of U_{max} versus photon energy plots in fluoride solutions from the expected value of unity has been attributed by Furtak and Macomber (14) to local potential variations. The same argument has also been used to explain the presence of unusual features in the electroreflectance spectra of silver single crystals in NaF (20). Furtak and Macomber (14) measured potential profiles of the totally symmetric ring breathing mode of pyridine in 0.5 M KF and found that the slope of their photon energy versus U_{max} plots was not

one but 1.46 eV/V. This can be compared with the slope for DABCO if one takes the inverse, since in the current work U_{max} has been plotted against photon energy; the resulting slope of 0.685 V/eV can be compared to the slope of the fluoride line in Figure 8, -0.692 V/eV. The signs are opposite because the direction of the charge transfer is opposite for the two sytems; otherwise the agreement is excellent. This suggests that a common origin underlies the deviation of the slope from one, and it is related to the fluoride ion rather than the adsorbed molecule; it is suggested that this is the local potential variations as first proposed by Furtak and Macomber (14). Since the charge transfer process involves two spatially separate states, these states will experience different electrostatic potentials in the inner layer, where the DABCO molecule is assumed to sit. The potential drop across the inner layer is usually described as being linear, but when the finite size of the water dipoles and the specifically adsorbed anions is taken into account, one finds an oscillatory behavior of the potential about the linearly-varying average value (21). As the applied potential is changed, there can be much larger variations of the potential drop at the surface, which will be important for those states at the surface which are involved in the charge transfer process. On the basis of their experimentally measured slope of 1.46, Furtak and Macomber suggest that the local field variations are 50% larger than the applied potential change.

This model can account for the deviation of the fluoride slope from unity, but still leaves open the question of the large difference between the fluoride slope and the perchlorate slope. Since both anions are only slightly adsorbed, why aren't the two slopes the same, with both giving rise to local potential variations? A tentative hypothesis is that the difference is a result of the size of the anions involved. Valette (22) invoked the anion size to explain the difference in the apparent order of specific adsorption of fluoride and perchlorate ions on silver (110) and (100) single crystal

faces; the order of increasing specific adsorption is:

(100) $PF_6^- < F^- < ClO_4^-$

(110) $PF_6^- < ClO_4^- < F^-$

This reversal was attributed to the much greater size of the perchlorate ion, which inhibits its penetration into the inner layer of the (110) face, this face being more rough on an atomic scale than the (100) face. The electrical behavior of the (110) face approaches that of the polycrystalline silver electrode (22), and this suggests that the order of the slopes of the perchlorate and fluoride data from the potential profiles might also be related to the size of the ion. Thus it is proposed that the local potential felt at the molecular site in the presence of the fluoride ion is greater than that felt in the presence of the perchlorate ion, simply due to the larger spatial extent of the latter which "spreads out" the potential variation over a greater distance. Naively assuming a linear potential variation across the ion, and that the potential variation is reflected directly by the slope of the lines in Figure 8, the ratio of these slopes may reflect the ion size difference. The ratio of the slopes is 1.53; Valette (22) calculated ionic diameters for fluoride and perchlorate ions at the silver (100) face of 0.3 and 0.53 nm respectively, from inner layer capacity studies, these values giving a ratio of 1.77. The closeness of these values may be fortuitous, but may also suggest the qualitative validity of the proposal. Certainly, the explanation of the deviation of the observed slopes from unity and the difference of the fluoride and perchlorate slopes will require a consideration of the microscopic structure of the double layer, and the texture of the surface.

The resonance condition $\hbar\omega_L = U_o + U_m$, implies that at zero photon energy $\hbar\omega_L$ the electrode potential $U_m = U_o$, the oxidation potential of the molecule (or the reduction potential if the direction of charge transfer is metal to molecule). Thus the intercepts listed in Table II should give the oxidation potential of DABCO on silver, esti-

mated to be +0.7 V vs SCE from experiments in acetonitrile at a rotating Pt electode (23). A serious problem is to decide which of the intercepts to use, since the lines in each electrolyte have very different slopes and intercepts. Because of the specific adsorption of chloride, the intercept in this electrolyte is probably a bad choice. This leaves the fluoride and perchlorate intercepts which give markedly different values of 1.08 V and 1.94 V respectively, the value in fluoride being closer to 0.7 V. This difficulty with the intercepts has been noted by Thietke et al., (19); one can easily see in their figures plotting photon energy versus U_m for the pyridine ring breathing mode, and in those of Furtak and Macomber (14), that extrapolation of the lines in different electrolytes yields very different values of the reduction potential of pyridine. Moreover, even with the same electrolyte, e.g., 0.1 M KCl, the values of the intercepts obtained vary from mode to mode for DABCO in the current work and for pyridine and pyrazine in the work of Thietke et al., (19). There is clearly much more work to be done in order to understand and quantify the behavior of the potential profiles.

Excitation Profiles: SERS excitation profiles present a greater challenge, both experimentally and in interpretation, than do the potential profiles. The difficulty in interpretation arises from the dependence of both terms $F_{EM}(\omega_L)$ and $F_{PDCT}(\omega_L)$ on ω_L, while the experimental difficulties arise from the need to scan each spectral region of interest at each excitation wavelength (thus giving rise to the same problems of time dependence found in the potential profiles) and from the need to use an intensity standard. No such standard was required for the potential profiles because once the cell was set up, only the electrode potential was varied while none of the optical parameters were altered. In the excitation profile measurements, the excitation wavelength was altered, thus giving rise to changes in the laser power and point of illumination, as well as variations in the response of the spectrometer and detector. In spite

of the obvious dangers of having an extra component present in the solution, the choice was made to use an internal standard to compensate for the aforementioned problems. The standard of choice was the perchlorate anion since this species has a strong Raman band at 935 cm^{-1}, and is not strongly specifically adsorbed on silver; however in order to verify that there was no interference from the internal standard several experiments were repeated using the nitrate ion as the internal standard. Nitrate ion has a strong Raman band at 1050 cm^{-1} which is also convenient for excitation profile measurements on DABCO, the region of interest being 750-1100 cm^{-1} where ν_5 and ν_4 lie; however, the nitrate ion is not as inert as the perchlorate ion although SERS of this species has rarely been reported (Wetzel et al., (24) report SERS of nitrate co-adsorbed with EDTA). It was thus expected that if the excitation profiles obtained using these two different internal standards agreed, there would be no problems arising from possible SERS of the standard itself.

Substantial concentrations of the standard were needed since at the low laser powers used (< 100 mW) unenhanced signals from bulk species were very weak and subject to the ν^4 law which resulted in reduced intensity when excitation in the red was used. The concentration of the standard used was therefore 0.9 M or greater but even at these high concentrations the signal obtained using the 676.4 nm line of the Kr^+ laser was very weak from the bulk standard, since at most 50 mW of laser power could be obtained from this line without the plasma line filter. This thus required the use of longer integration times with a consequent increase in the possibility of laser-induced damage to the surface. The low intensity of the 676.4 nm Krypton laser line gave data obtained using this exciting line a large uncertainty. A further problem encountered was the low number of laser exciting lines between 514.5 nm and 647.1 nm, namely only one at 568.2 nm; clearly a tunable dye laser would be more suitable for this work, but in its absence the best was made of the available lines.

The standard used for most of the work was 0.9 M sodium perchlorate, since the potassium salt is not sufficiently soluble , and the solution was made 0.1 M in sodium chloride to make the roughening procedure more reproducible. In some experiments 2.0 M sodium perchlorate with 0.1 M sodium chloride was used; no significant differences were observed between the excitation profiles measured using this standard and the more dilute standard. The raw areas thus obtained were then normalized using the following procedure. All of the perchlorate band intensities were normalized to that of the perchlorate intensity at one wavelength, $I^{ClO_4^-}_{\lambda^o}$. In this way a set of normalizing factors N_λ were obtained

$$N_\lambda = \frac{I^{ClO_4^-}_{\lambda^o}}{I^{ClO_4^-}_{\lambda}}$$

and these N_λ were then used to scale the measured SERS intensities of the band of interest, I^m_λ,

$$I^S_\lambda = N_\lambda \cdot I^m_\lambda$$

to give the scaled integrated intensity I^S_λ.

There are four SERS bands which lie in the region 750-1100 cm^{-1} which are detectable at all excitation wavelengths; of these, ν_4 and ν_5 are strong while ν_{10} and ν_{18} are weak but still above the noise level at all wavelengths used. The excitation profile data are plotted in Figure 9, where the non-coincidence of the maxima is apparent in spite of the low number of laser lines available. It appears that ν_5, ν_{10} and ν_{18} maximize at about the same wavelength, and that ν_4 maximizes at a wavelength to the red of the other mode. The data plotted for ν_4 are the average of the result of three experiments, two in which perchlorate was the internal standard and one in which the standard was the nitrate ion. The excitation profiles measured with

nitrate and with perchlorate are very similar, the difference being within the 50 nm variation observed for profiles measured with the same standard. It is therefore concluded that the excitation profiles are independent of the internal standard, i.e., there is no SERS of the internal standard.

Before discussing the origin of the non-coincidence of the maxima in Figure 9, it is essential to decide whether EM or PDCT resonances are being observed. The answer to this question is to be found in the behavior of the maxima with changes in the electrode potential, since it has been assumed that the position of the EM resonance should be independent of the electrode potential while the PDCT resonance should shift in accord with the resonance condition given for the potential profiles. Therefore, excitation profiles were measured at a number of electrode potentials, chosen to be about 200 mV apart so that the shift of the maximum would be large enough to be detected. These experiments were carried out with the DILOR spectrometer using the multichannel detector, thus making it possible to do the entire experiment on the same electrode surface with short laser exposure time. In order to rule out any effects from the EM mechanism, measurements at some potentials were repeated on electrodes roughened using different ORCs, and thus different amounts of large scale roughness. The results of these experiments as the logarithm of the normalized areas are plotted in Figure 10 and Figure 11. The observed shift in the wavelength of maximum intensity λ_{max} with potential strongly suggests that the observed resonance in the excitation profiles arises from the PDCT mechanism.

This conclusion is further bolstered if one compares the direction of the shift of the excitation profile as the electrode potential is made more negative with the direction of the shift of the potential profile maximum as the excitation wavelength is made longer; i.e., the two sets of profiles are measuring the same phenomenon. A plot of the electrode potential versus the photon energy of the maximum of the reso-

nance is given in Figure 12. In spite of the small number of data points, a least squares fit to the data gave a good fit and a slope of -1.04, very close to the expected slope of minus one. That the effect of large scale roughness is negligible is apparent from the near coincidence of the two curves shown in Figure 10, measured at the same electrode potential (-850 mV) but where the electrode was roughened with two different ORCs. While there is a small shift (about 50 nm), this shift is not as large as that observed when the electrode potential is varied, where a shift of about 150 nm is observed with a 600 mV change in the electrode potential. While this does not definitely rule out a contribution from the EM mechanism to these resonances, the near coincidence of the two excitation profiles suggests that the large shifts which occur with changes in the electrode potential arise only from the PDCT contribution to the enhancement.

Interestingly, the excitation profiles exhibit an intensity variation of only one to two orders of magnitude at any given wavelength; i.e., the SERS intensity is only one to two orders of magnitude greater "on-resonance" than "off-resonance". This variation is the same as that observed for the potential profiles as discussed in the previous section. This suggests that the total contribution from the PDCT mechanism is one to two orders of magnitude. One can also see from Figure 10 and Figure 11 that the overall enhancement both on and off resonance is greater at longer wavelengths. This probably reflects a change in the EM enhancement, the latter becoming greater as the excitation wavelength is made longer. It is therefore suggested that the observed excitation profiles are a superposition of two separate excitation profiles. One of these profiles, due to the EM mechanism, is potential independent but roughness dependent, and increases as the excitation wavelength is made longer. The other excitation profile is the potential-dependent resonance due to the PDCT mechanism.

Excitation profiles have not been reported in the literature for very many electrochemical systems, and there is only one report of a systematic measurement of these curves as a function of the electrode potential, in the recent work of Lin and Chou (25). They measured the excitation profiles of four bands of pyridine adsorbed on a silver electrode in 0.1 M NaCl, 1 M $NaClO_4$, 0.01 M pyridine. They observed maxima in some of the excitation profiles which they attributed to a voltage-dependent charge-transfer resonance, superimposed on a voltage-independent contribution from the EM mechanism. The EM contribution exhibited a monotonic increase with excitation wavelength. They also suggested that a change in the pyridine orientation occurred, which also contributed to the excitation profile. The direction of the shift of the resonant maxima upon making the electrode potential more cathodic was toward longer wavelengths, in agreement with a PDCT model in which the direction of the charge transfer is from the metal to the molecule. This is the same direction of charge transfer deduced from the potential profile measurements; for example, see the work of Billmann and Otto (2). The results of the excitation profiles of DABCO are very similar to those of Lin and Chou (25) except for the opposite direction of the shift of the resonances because of the opposite direction of the charge transfer for DABCO. Other earlier excitation profile measurements on electrode surfaces did not include a study of the potential dependence. Pettinger et al., (26) and Pettinger and Wetzel (27) reported the excitation profile of the 1008 cm^{-1} band of pyridine at a silver electrode, finding a maximum at wavelengths longer than 600 nm. Blatchford et al., (28) measured the excitation profiles of cyanide ion, deuterated pyridine, triphenylphosphine and ruthenium red at electrochemically roughened electrodes and found that for each of these molecules there is a maximum in the excitation profile between 580 and 720 nm. These profiles were found to depend slightly upon the ORC used in the roughening procedure, shifts being on the order of 50 nm. These excitation profile measure-

ments may reflect mainly the EM contribution, giving a maximum at wavelengths longer than 600 nm. There is clearly more work that could be done in this area; the variation of the excitation profile with the electrode roughening procedure needs to be studied; the study should be redone with a dye laser in order to fill in the gaps in the excitation profiles. As well, it would be interesting to study the effect of the supporting electrolyte on the excitation profile, since such an effect was found for the potential profiles.

Returning now to the non-coincidence of the excitation profiles of different DABCO modes (Figure 9), it is likely that this is in part due to the differing degrees of PDCT enhancement experienced by the various modes. ν_4, the C-C totally symmetric stretch, is the mode which is expected to show the greatest amount of PDCT enhancement (1), and its excitation profile is the one which is shifted from the others. There may also be a contribution from the differences in the behavior of the normal and tangential fields at the surface. Because the normal field becomes greater than the tangential field at longer wavelengths (29), the C-C stretch would be expected to become relatively more intense at longer wavelengths if the DABCO molecule were oriented with the N-N axis along the surface normal. The C-N totally symmetric stretch, ν_5, is a more isotropic mode as evidenced by its depolarization ratio and thus at shorter wavelengths, where both normal and tangential fields are strong, this mode would be relatively more intense than at longer wavelengths where only the α_{zz} component can scatter.

DABCO Band Frequencies.

The band frequencies of the four strongest SERS bands (ν_3, ν_4, ν_5, and ν_6) for DABCO adsorbed on a silver electrode in 0.1 M KCl, 0.05 M DABCO are given in Table III as a function of the electrode potential; these band frequencies are accurate

to within 0.5 cm^{-1}. For easy comparison, the band shifts $\Delta\nu = \nu - \nu_{150}$, where ν is the band frequency at the given potential and ν_{150} is the band position at -150 mV, are plotted in Figure 13. One can see that the three bands ν_3, ν_4 and ν_6 exhibit large downward shifts in frequency (up to 14 cm^{-1}) as the electrode potential is made more negative, while ν_5 is observed to shift by only about 2 cm^{-1}. This behavior can be compared with the behavior of the same four bands with changes in solvent and with pH changes (30, 31); the frequencies of ν_3, ν_4, and ν_6 are sensitive indicators of the extent of the interaction of the DABCO lone pairs (e.g., via hydrogen bonding or protonation); the frequency of ν_5 was found to be only weakly altered by these same interactions. The direction of these shifts was to higher frequency with increasing interaction strength. Since the frequencies of ν_3, ν_4, and ν_6 in the SER spectrum at -150 mV are higher than their counterparts in aqueous solution, this indicates a strong DABCO-surface interaction via the lone pair on one of the nitrogen atoms at this potential. The interaction weakens with increasing negative potential, as reflected in the decrease in the band frequencies as the potential is made more negative. This weakening of the interaction can easily be understood; at a potential of -150 mV, the electrode is positively charged, thus allowing a strong interaction with the electron rich lone pairs. As the electrode potential is made more negative, the electrode charge becomes less positive until the point of zero charge (pzc) is reached. This potential is about -900 mV on silver in the absence of specific adsorption; at potentials more negative than the pzc, the electrode will have a negative charge.

Further evidence that this is the correct interpretation of the band shifts comes from experiments in which the position of ν_4 was measured in solutions 0.05 M in DABCO and 0.1 M in different supporting electrolytes. Four supporting electrolytes were chosen, these being sodium fluoride, sodium perchlorate, potassium chloride and

potassium bromide. The specific adsorption of anions is known to shift the point of zero charge (32). Measurements of the frequency of ν_4 in 0.05 M DABCO + 0.5 or 1.0 M KCl were also carried out to investigate the dependence of the band frequency on the bulk concentration of the anion. The results of these measurements are listed in Table IV and plotted in Figure 14; in this figure the actual band frequency is plotted versus the electrode potential, rather than a frequency difference. As anticipated, the band position does depend upon the identity of the anion and its bulk concentration, in a manner which is consistent with the changes in the electrode charge expected when specific adsorption occurs. The band frequencies in perchlorate- and fluoride-containing solutions are identical within the experimental error over most of the potential range measured, diverging only at the most anodic potentials. Both of these anions are only weakly specifically adsorbed on silver, perchlorate being slightly more adsorbing than fluoride , and this is reflected in the band positions at anodic potentials. Over most of the potential range more negative than -300 mV, the band frequency of ν_4 in both electrolytes are the same and this band frequency is related to the strength of the DABCO-surface interaction **in the absence** of specific adsorption. The changes in the band frequency in chloride and bromide electrolytes are similar to those in fluoride and perchlorate except that they are shifted to more cathodic potentials and the rate of decrease of the band frequency is greater. That is, a given frequency for ν_4 occurs at an increasingly cathodic potential in the order

less cathodic $\quad ClO_4^-,\ F^- < Cl^- < Br^-$ $\quad$ *more cathodic*

. As well, the variation in the band frequency in going from 0.1 M KCl to 1.0 M KCl is in the order

less cathodic $\quad 0.1M < 0.5M < 1.0M$ $\quad$ *more cathodic*

.

All of the curves in Figure 14 appear to converge to the same value at the most negative potentials, that value being $980 \pm 1 cm^{-1}$ at -1200 mV. At this potential all of the anions should be desorbed, and the convergence of the curves is therefore reasonable. It is interesting that the band frequency of ν_4 at -1200 mV is lower than the band frequency of this band in aqueous solution, 983 cm^{-1} , suggesting that the DABCO molecule is still interacting slightly with the surface even when the surface is negatively charged. This is in accord with differential capacity measurements which indicate that at 0.05 M DABCO concentrations the molecule is adsorbed at potentials out to hydrogen evolution. The SERS signals obtained at these potentials are rather weak although still observable, and it is proposed that the EM enhancement only is operative in this potential region. Since the magnitude of the PDCT mechanism will depend in some manner (no quantitative predictions possible) on the extent of the DABCO surface interaction, the weak interaction at -1200 mV as indicated by the low frequency of ν_4 also suggests that the PDCT mechanism is weak at these potentials.

Returning to the changes in the frequency of ν_4 with anion changes, the observed behavior can be readily understood as reflecting the shift in the electrode charge $\delta\sigma_m$ at constant electrode potential caused by the specific adsorption of anions, analogous to the shift in the potential profiles with anion noted. Unlike the potential profiles, the band frequency is somewhat easier to study and it was possible to attempt to quantify the observed shifts. Consider the frequency of ν_4 at constant electrode potential, for example -500 mV. At this potential the frequency of this band decreases in the order

$$Br^- > 1.0 M Cl^- > 0.5 M Cl^- > 0.1 M Cl^- > F^-,\ ClO_4^-$$

where the frequency of the band in fluoride- or perchlorate-containing solutions is assumed to represent the band position in the absence of specific adsorption. The effect of specific adsorption is to shift σ_m to more positive values at constant electrode potential (32). Making the electrode more positive will strengthen the DABCO lone-pair-surface interaction and shift ν_4 to higher frequency, as observed. The order of the extent of specific adsorption for halides is

$$Br^- > Cl^- > F^-$$

which is the same ordering as observed for the shift in ν_4. The bulk concentration of the anion has a similar effect, higher bulk concentrations leading to greater adsorption and thus to greater $\Delta\sigma_m$. This concentration-dependent shift can be quantified. For a bulk concentration of anion c and at constant cation concentration , the shift in σ_m at constant electrode potential is proportional to ln(c) at low values of c; the validity of this relationship for low concentrations of bromide and chloride on silver has been shown by Valette (32). In spite of the high concentrations of anion used in the SERS experiments and the varying cation concentration, it was of interest to see if the DABCO band shifts, assumed to be related to $\Delta\sigma_m$, fit this relationship. It was therefore assumed that a simple linear relationship exists between the band position of ν_4 and the electrode charge σ_m. The electrode charge shift at constant electrode potential and at chloride concentration x, $\Delta\sigma_m^x$ is therefore

$$\Delta\sigma_m^x = \Delta\nu_x = \nu_x - \nu_o$$

where ν_x is the frequency of ν_4 at a chloride concentration of x M, and ν_o is the frequency of ν_4 in the absence of specific adsorption, taken from the fluoride or perchlorate curves. The data obtained from this analysis are listed in Table V and $\Delta\nu_x$ versus ln(c) is plotted in Figure 15. Considering the 0.5 cm^{-1} error in the band positions,

the rather high concentrations of anion and the limited number of points available, the fairly linear relationship observed suggests the correctness of the argument that the DABCO band shifts arise as a result of the changes in the DABCO-surface interaction due to the surface charge changes caused by the specific adsorption of anions. It would be interesting to extend these experiments by including more concentrations and going to lower concentrations, but the band shifts are not large enough to make this feasible.

Conclusions.

In this study we have shown that the SER spectra of the DABCO molecule adsorbed on the surface of a silver electrode can be explained by the assumption that the total observed enhancement arises from both an electromagnetic enhancement and a PDCT enhancement, the latter accounting for about one to two orders of magnitude of the total. On the basis of the observed shifts of the potential and excitation profiles the direction of the charge transfer must be from the molecule to the metal, as proposed previously (10). As well as this excited state charge transfer, there is in addition a ground state charge transfer which results in a shift of the band frequencies of the DABCO molecule, and which changes with the electrode potential.

Acknowledgements.

This work was supported by grants from the Natural Sciences and Engineering Research Council of Canada and the Office of Naval Research (USA). D.A.G. is grateful for the award of an Ontario Graduate Scholarship.

References

1. Moskovits, M. Rev. Mod. Phys. 1985, 57, 783.

2. Otto, A. In "Light Scattering in Solids IV", M. Cardona and G. Guntherodt, Eds., Topics in Applied Physics, Springer: Berlin, 1984; vol 54.

3. Burstein, E.; Chen, Y.J.; Chen, C. Y.; Lundquist, S.; Tosatti, E. Solid State Commun., 1979, 29, 567.

4. Gersten, J.I.; Birke, R.L.;, Lombardi, J.R. Phys. Rev. Letters, 1979, 43, 147

5. Persson, B. Chem. Phys. Lett. 1981, 82, 561.

6. Ueba, H. In "Surface Enhanced Raman Scattering", R.K. Chang and T.E. Furtak Eds; 1982, Plenum, New York, 1982; p.173

7. Adrian, F.J. J. Chem. Phys. 1982, 77, 5302.

8. Arya, K.; Zeyher, R. Phys. Rev. B 1981, 24 1852.

9. Otto, A.; Pockrand, I.; Billmann, J.; Pettenkoffer, C. In "Surface Enhanced Raman Scattering", R. K. Chang and T. E. Furtak, Eds; Plenum, New York, 1982; p.173.

10. Irish, D. E.;Guzonas D. A.; Atkinson, G. F. Surface Sci. 1985, 158, 314.

11. Heilbronner, E.; Muszkat, K. A. J.Am. Chem. Soc. 1970, 92, 3818.,

12. Halpern, A. M.; Weiss, K. J. Am. Chem. Soc. 1970, 90, 6297.

13. Billman, J.; Otto, A. Solid State Commun. 1982, 44, 105.

14. Furtak, T. E.; Macomber, S. H. Chem. Phys. Lett. 1983, 95, 328.

15. Murphy, W. F.; Bernstein, H. J. J. Phys. Chem. 1972, 76, 1147.

16. Santos, P. S.; Mello, M. T. S.; J. Mol. Struct. 1988, 178, 121.

17. Ernstbrunner, E. E.; Girling, R. B.; Grossman, W. E. L.; Hester , R. E. J.C.S. Faraday II, 1978, 74, 501.

18. Jeanmaire, D. L.; Van Duyne, R. P. J. Electroanal. Chem. 1977, 84, 1.

19. Thietke, J.; Billman, J.; Otto, A. Proc. 17th Jerusalem Symposium in Quantum Chemistry and Biochemistry. Int. Symp. on Dynamics on Surfaces B. Pullman, J. Jortner, and D. Reidel Eds; 1985.

20. Kolb, D. M.; Boeck, W.; Ho, K. M.; Liu, S. H. Phys. Rev. Lett. 1981, 47, 1921.

21. Carnie, S. L.; Chan, D. Y. C. J. Chem. Phys. 1980, 73, 2949.

22. Valette, G. J. Electroanal. Chem. 1981, 122, 285.

23. McKinney, T. M.; Geske, D. H. J. Am. Chem. Soc. 1965, 87, 3013.

24. Wetzel, H.; Pettinger, B.; Wenning, J. Chem. Phys. Lett. 1980, 75, 173.

25. Lin, H. J.; Chou, Y. C. Chem. Phys. Lett. 1986, 125, 53.

26. Pettinger, B.; Wenning, U.; Kolb, D. M. Ber. Bunsenges. Physik. Chem. 1978, 82, 1326.

27. Pettinger, B.; Wetzel, H. in " Surface Enhanced Raman Scattering " R. K. Chang and T. E. Furtak, Eds. Plenum Press, New York, 1982; p.293.

28. Blatchford, C. G.; Campbell, J. R.; Creighton, J. A. Surface. Sci. 1981, 108, 411.

29. Moskovits, M.; Suh, J. S. J. Phys. Chem. 1984, 88, 5526.

30. Guzonas, D. A.; Irish, D. E.; Can. J. Chem. 1988, 66, 1249.

31. Guzonas, D. A.; Irish, D. E.; Atkinson, G. F. Langmuir 1989, 5, 787.

32. Valette, G. J. Electroanal. Chem. 1983, 146, 439.

FIGURE CAPTIONS

Figure 1. Schematic diagram of the photon-driven charge-transfer model for the surface enhancement of the DABCO molecule. The four step process involves 1) creation of an e-h pair in the metal, 2) tunneling of the hole from the metal to the molecule, 3) tunneling of the hole back to the metal, and 4) recombination to give emitted photon.

Figure 2. The SER (upper) and normal Raman (bottom) spectra of DABCO The SER spectrum was recorded at -500 mV on a silver electrode using 568.2 nm excitation, the normal Raman spectrum is of a 2 M solution of DABCO excited by 514.5 nm radiation.

Figure 3. The Raman spectrum of the DABCO-iodine charge transfer complex. The spectrum was obtained using 20 mW of 568.2 nm excitation under the 100x objective of the OMARS-89.

Figure 4. Rapid-scan of the ν_4 line of DABCO illustrating the dependence of the SERS intensity maxima on the excitation wavelength. The spectra were scanned at 2.5 cm^{-1}/s. Between each set of scans at different wavelengths the electrode was repolished and reroughened. Note the change in scale for the most cathodic spectra at 647.1 nm.

Figure 5. SERS potential profiles of DABCO adsorbed on a silver electrode in 0.1 M perchlorate supporting electrolyte.

Figure 6. The SERS potential profiles of ν_4 of DABCO adsorbed on silver in the presence of three different supporting electrolytes.

Figure 7. A plot of the potential of the maximum intensity of the potential profiles versus the excitation photon energy.

Figure 8. A plot of the potentials of the maximum intensity of the potential profiles of ν_4 versus the excitation photon energy for three supporting electrolytes.

Figure 9. The SERS excitation profiles for four DABCO modes.

Figure 10. The shift of the excitation profile of ν_4 with applied potential.

Figure 11. The shift of the excitation profile of ν_5 with applied potential.

Figure 12. A plot of the electrode potential versus the photon energy at the maximum of the excitation profiles.

Figure 13. The relative band frequencies of the four strongest DABCO bands as a function of the electrode potential. The crosses are ν_5, the asterisks ν_6, the triangles ν_4 and the open circles ν_3.

Figure 14. The variation of the frequency of ν_4 with electrode potential in different supporting electrolytes. The open circles are the perchlorate data, the plusses are the fluoride data, the triangles, crosses and filled circles are the data for 0.1, 0.5 and 1.0 M chloride, respectively, and the asterisks are the data for 0.1 M bromide.

Figure 15. The change in the frequency of ν_4 versus the logarithm of the anion concentration. The open circles, crosses, pluses and triangles are the data points for -500, -550, -600 and -700 mV, respectively.

Tables

Table 1: Values of the potential of the intensity maxima of four DABCO bands versus excitation wavelength.

		MODE NUMBER			
		ν_3	ν_4	ν_5	ν_6
excitation wavelength /nm	excitation energy /eV	Intensity maximum /mV			
647.1	1.919	-340	-430	-368	-482
568.2	2.186	----	-550	----	----
514.5	2.414	-490	-620	-535	-630
501.7	2.466	-496	-705	-544	-630
488.0	2.545	-580	----	-586	-682
457.9	2.702	----	-820	----	----
slope		-0.338	-0.489	-0.337	-0.300
intercept		0.312	0.518	0.277	0.093
r		0.963	0.986	0.996	0.988

Table 2: Potentials of maximum intensity of ν_4 as a function of excitation wavelength in two electrolytes

Excitation Wavelength /nm	Excitation Energy /eV	Electrode Potential sodium fluoride /mV	Electrode Potential sodium perchlorate /mV
676.4	1.829	-180	-35
647.1	1.919	-270	-70
568.2	2.186	-400	-335
514.5	2.414	-600	-600
488.0	2.545	----	-730
457.9	2.702	----	-950
slope		-0.692	-1.06
intercept		1.08	1.94
r		0.990	0.997

Table 3: Band Frequencies and shifts of the Four Strongest Bands of DABCO for different electrode potentials

Electrode Potential (mV)	Band frequency and Band shift (cm^{-1})							
	ν_3	$\Delta\nu_3$	ν_4	$\Delta\nu_4$	ν_5	$\Delta\nu_5$	ν_6	$\Delta\nu_6$
-150	1357.4	0.0	992.2	0.0	798.6	0.0	627.0	0.0
-200	1357.0	-0.4	992.6	+0.4	797.7	-0.9	627.0	0.0
-250	1356.5	-0.9	992.2	0.0				
-300	1355.5	-1.9	992.6	+0.4	798.0	-0.6	626.4	-0.6
-350	1354.5	-2.9	991.5	-0.7	797.2	-1.4		
-400	1352.7	-4.7	990.8	-1.4	797.2	-1.4	624.7	-2.3
-450	1351.7	-5.7	989.8	-2.4	796.9	-1.7		
-500	1350.9	-6.5	989.1	-3.1	796.9	-1.7	623.0	-4.0
-550	1349.1	-8.3	987.3	-4.9	796.9	-1.7		
-600	1348.6	-8.8	986.6	-5.6	796.6	-2.0	622.5	-4.5
-650	1346.8	-10.6	985.3	-6.9				
-700	1346.7	-10.7	983.8	-8.4	796.1	-2.5	620.8	-6.2
-800	xxxx.x	xx.x	982.4	-9.8	xx.x	xx.x	619.1	-7.9
-900	1342.9	-14.5	981.0	-11.2	797.7	-0.9	620.8	-6.2
-1000	xxxx.x	xx.x	980.6	-11.6				
-1100	xxxx.x	xx.x	979.6	-12.6				

xxxx - not measured

Table 4: The band frequencies of the CC stretch as a function of the electrode potential in different supporting electrolytes

Electrode Potential (mV)	Supporting Electrolyte					
	$NaClO_4$	NaF	KCl 0.1M	KCl 0.5M	KCl 1.0M	KBr
-100	993.2	990.7				
-150	992.6		992.2			
-200	992.8	991.3	992.6			
-250	991.0		992.2			
-300	991.0	990.0	992.6	993.4		
-350	989.3		991.5	994.0		
-400		988.8	990.8	993.3		
-450	987.4		989.1	991.9		
-500	986.9	986.9	989.1	991.2	992.0	994.2
-550	985.8		987.3	989.5		994.2
-600		986.4	986.6	987.7	989.7	993.3
-650	984.4		985.3	986.8	989.2	992.4
-700	983.8	984.1	983.8	986.0	988.1	990.8
-750	983.2			985.1	986.4	988.9
-800		983.0	982.4	984.4	986.0	987.5
-850				984.1		986.3
-900	981.9	981.6	981.0	983.0	983.3	984.9
-950	981.0			982.0		982.9
-1000		981.7	980.6	981.5	980.9	980.7
-1050						980.7
-1100			979.6	980.3	980.1	980.7
-1200	980.2	980.5	978.5	979.4	979.3	980.7

Band frequencies are in cm^{-1}

Table 5: The change in CC band frequency at constant electrode potential as a function of chloride concentration

Electrode Potential	Band Frequency				Band Shift $\Delta\nu_z$		
	ν_o	$\nu_{0.1}$	$\nu_{0.5}$	$\nu_{1.0}$	$\Delta\nu_{0.1}$	$\Delta\nu_{0.5}$	$\Delta\nu_{1.0}$
-500	986.9	989.0	991.2	992.0	2.2	4.3	5.1
-550	986.0	987.5	989.5	990.9	1.5	3.5	4.9
-600	985.4	986.4	988.1	990.0	1.0	2.7	3.6
-700	983.9	983.9	986.1	988.1	0.0	2.2	4.2

Band Frequencies are in cm^{-1}

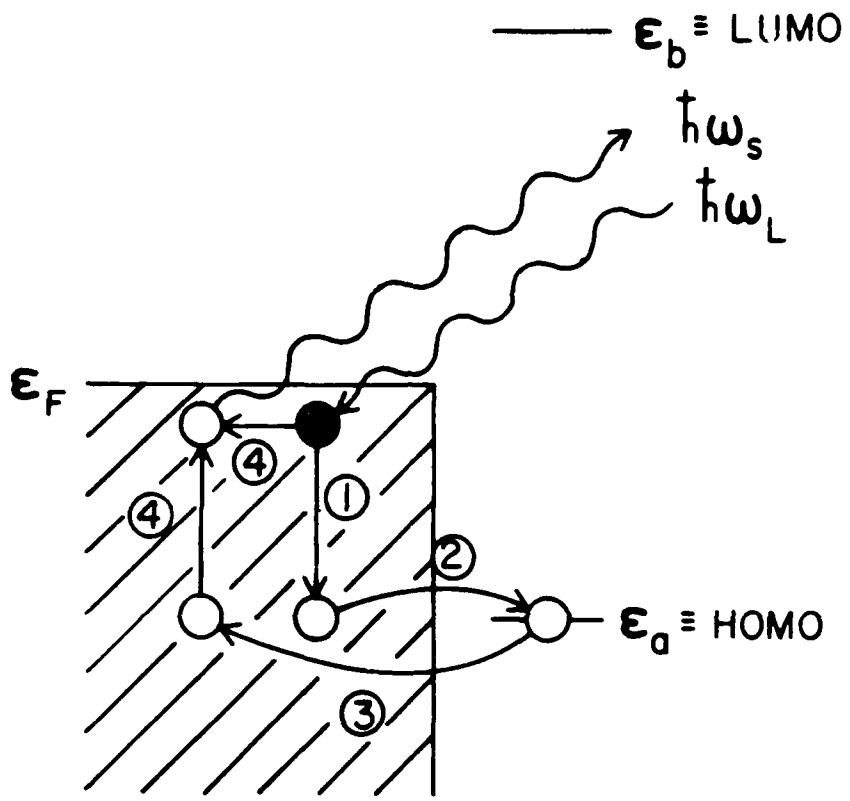

Figure 1. Schematic diagram of the photon-driven charge-transfer model for the surface enhancement of the DABCO molecule. The four step process involves 1) creation of an e-h pair in the metal, 2) tunneling of the hole from the metal to the molecule, 3) tunneling of the hole back to the metal, and 4) recombination to give emitted photon.

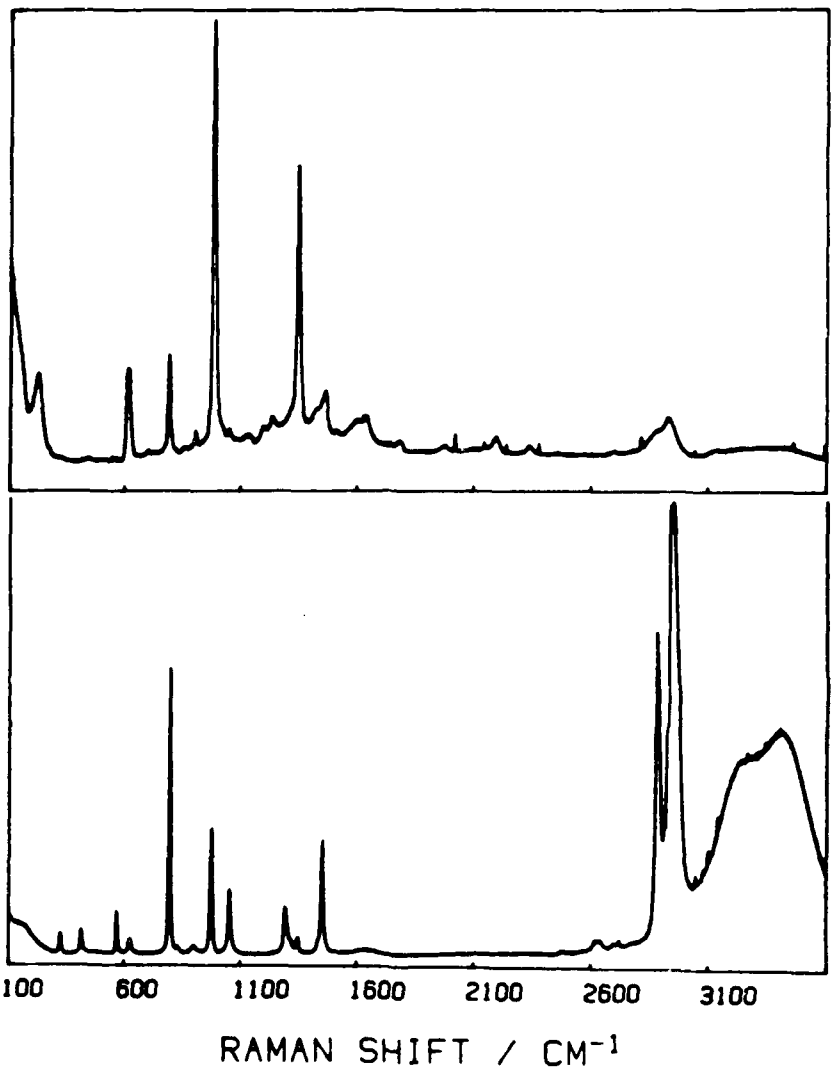

Figure 2. The SER (upper) and normal Raman (bottom) spectra of DABCO The SER spectrum was recorded at -500 mV on a silver electrode using 568.2 nm excitation, the normal Raman spectrum is of a 2 M solution of DABCO excited by 514.5 nm radiation.

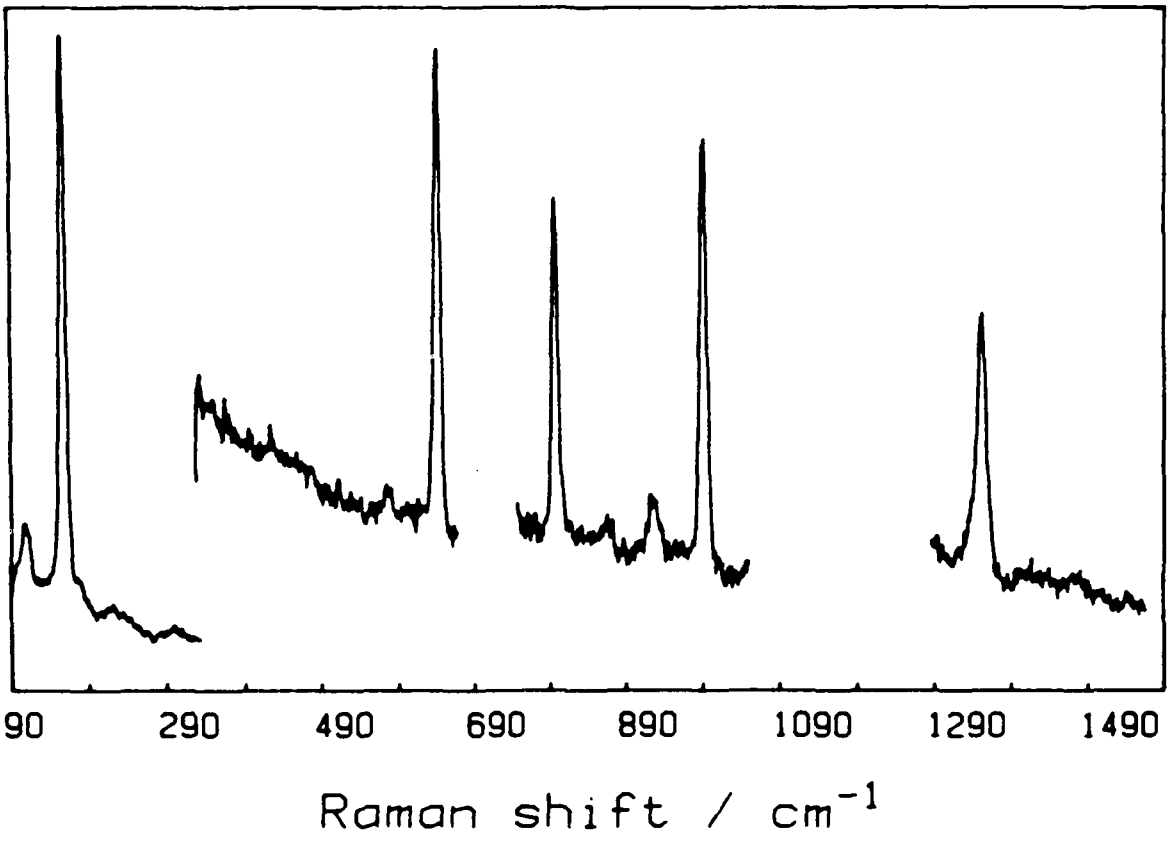

Figure 3. The Raman spectrum of the DABCO-iodine charge transfer complex. The spectrum was obtained using 20 mW of 568.2 nm excitation under the 100x objective of the OMARS-89.

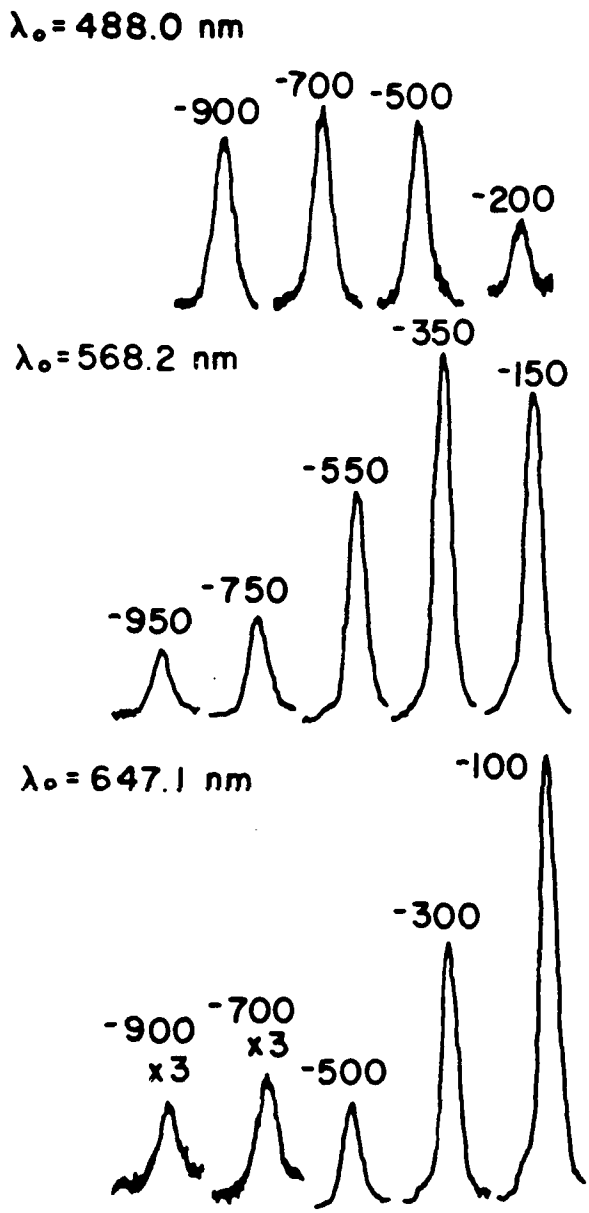

Figure 4. Rapid-scan of the ν_4 line of DABCO illustrating the dependence of the SERS intensity maxima on the excitation wavelength. The spectra were scanned at 2.5 cm^{-1} /s. Between each set of scans at different wavelengths the electrode was repolished and reroughened. Note the change in scale for the most cathodic spectra at 647.1 nm.

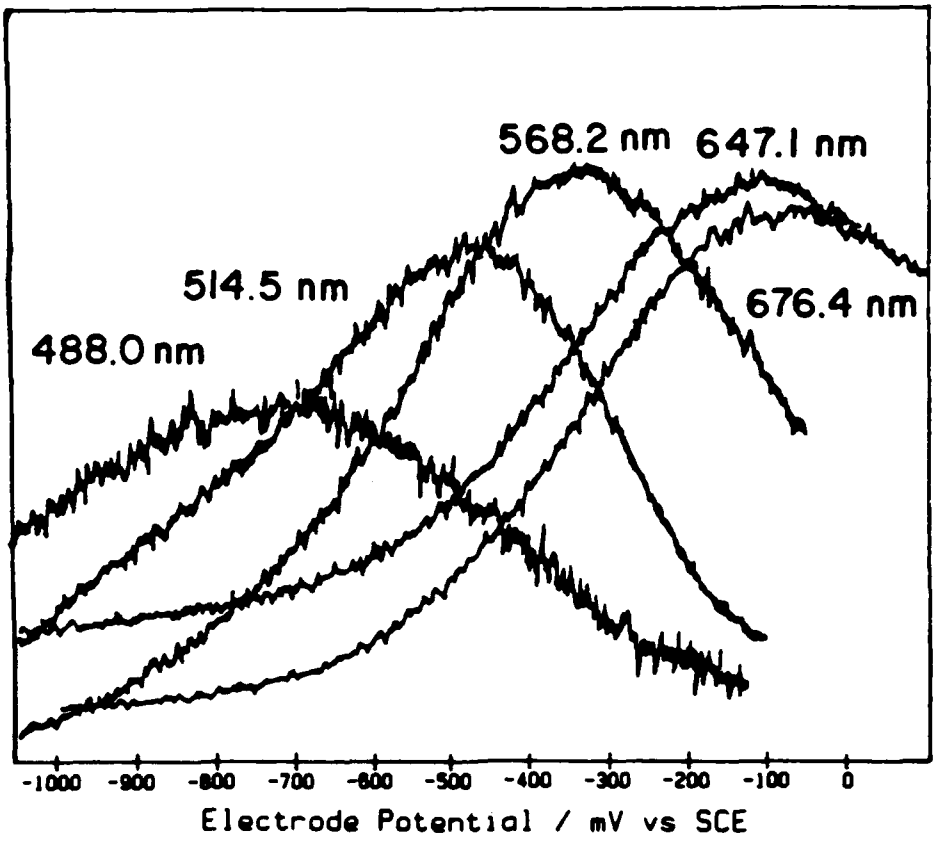

Figure 5. SERS potential profiles of DABCO adsorbed on a silver electrode in 0.1 M perchlorate supporting electrolyte.

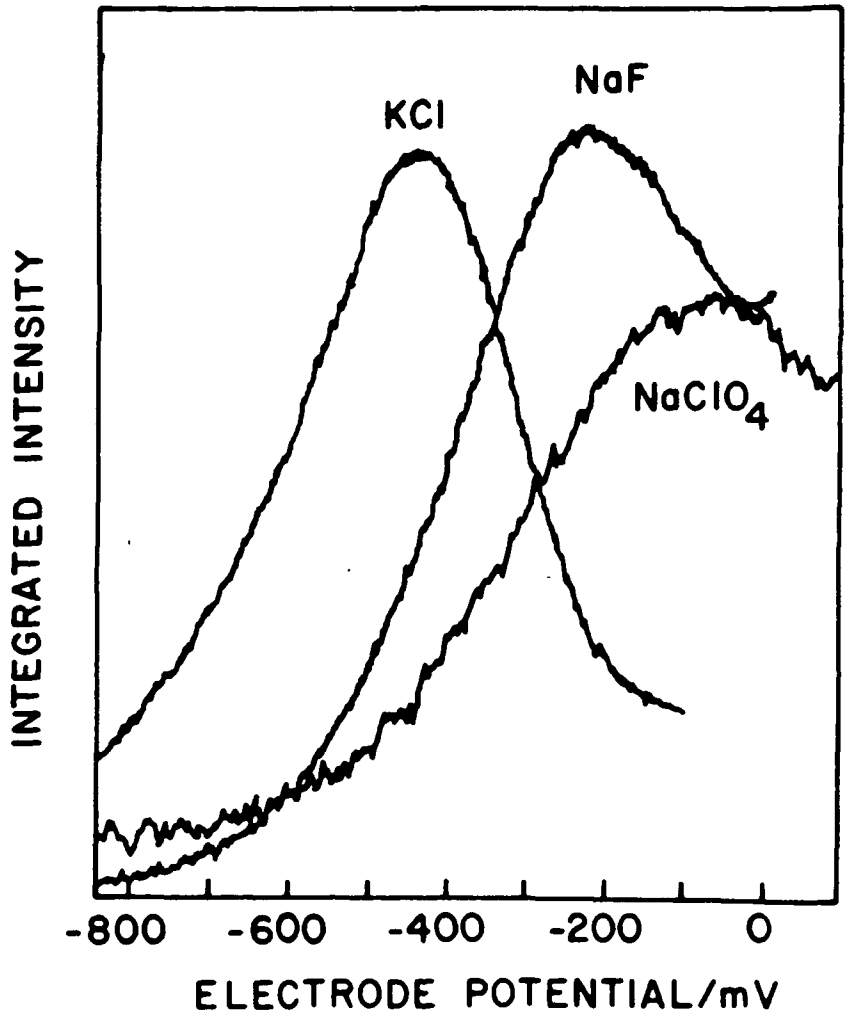

Figure 6. The SERS potential profiles of ν_4 of DABCO adsorbed on silver in the presence of three different supporting electrolytes.

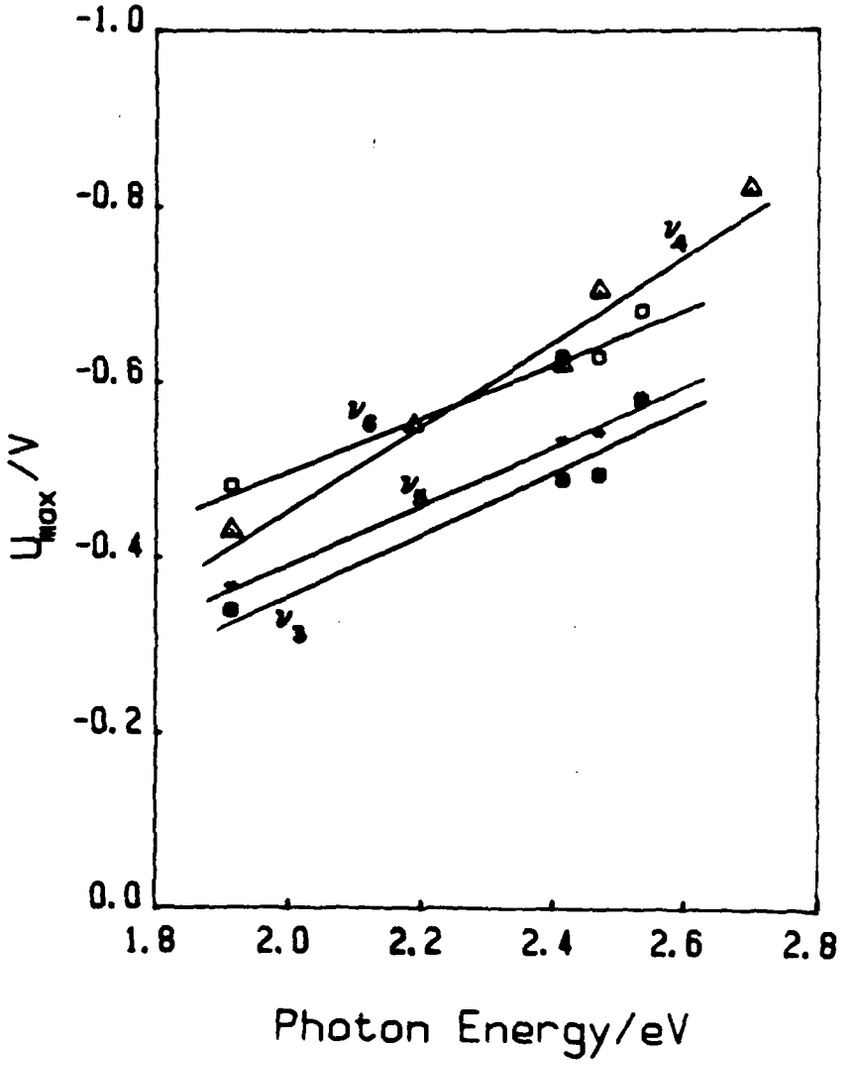

Figure 7. A plot of the potential of the maximum intensity of the potential profiles versus the excitation photon energy.

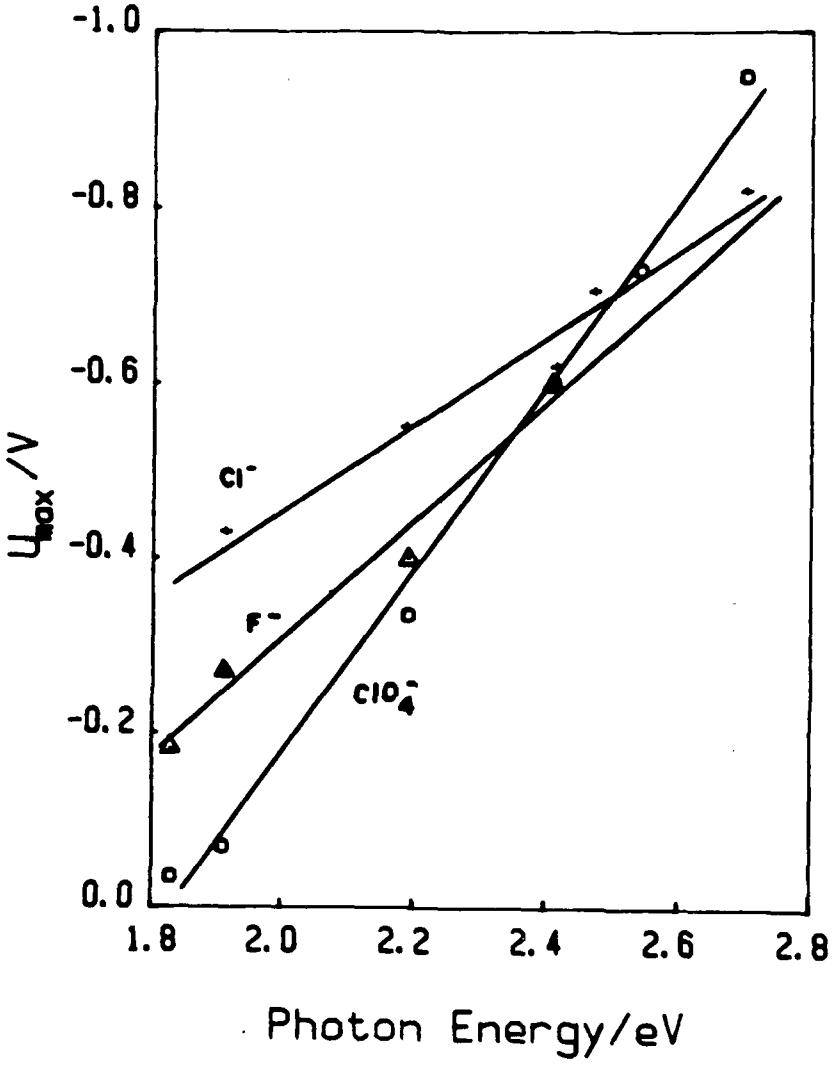

Figure 8. A plot of the potentials of the maximum intensity of the potential profiles of ν_4 versus the excitation photon energy for three supporting electrolytes.

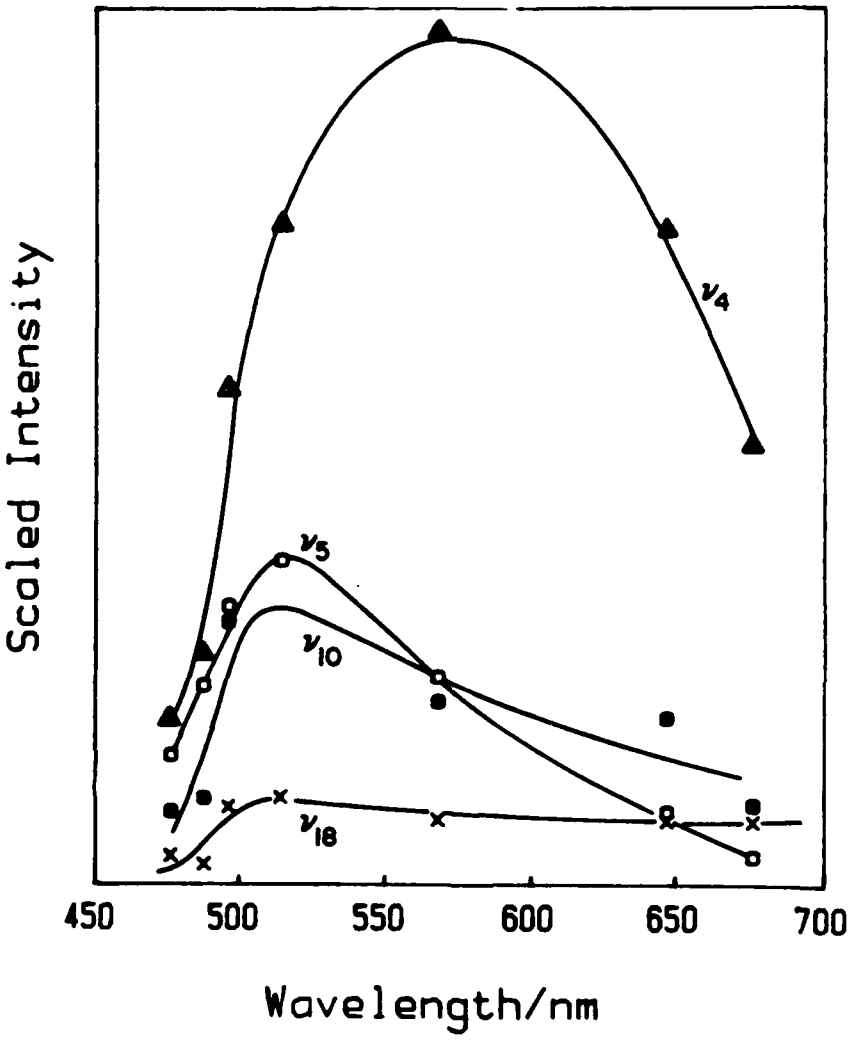

Figure 9. The SERS excitation profiles for four DABCO modes.

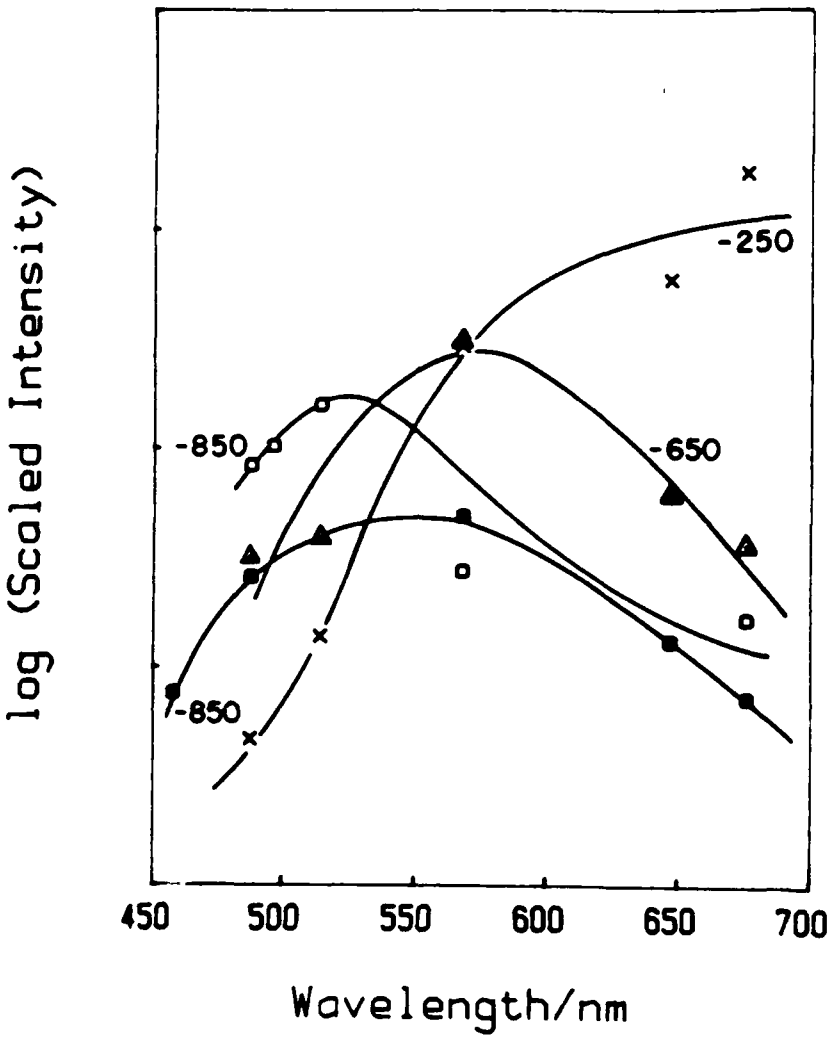

Figure 10. The shift of the excitation profile of ν_4 with applied potential.

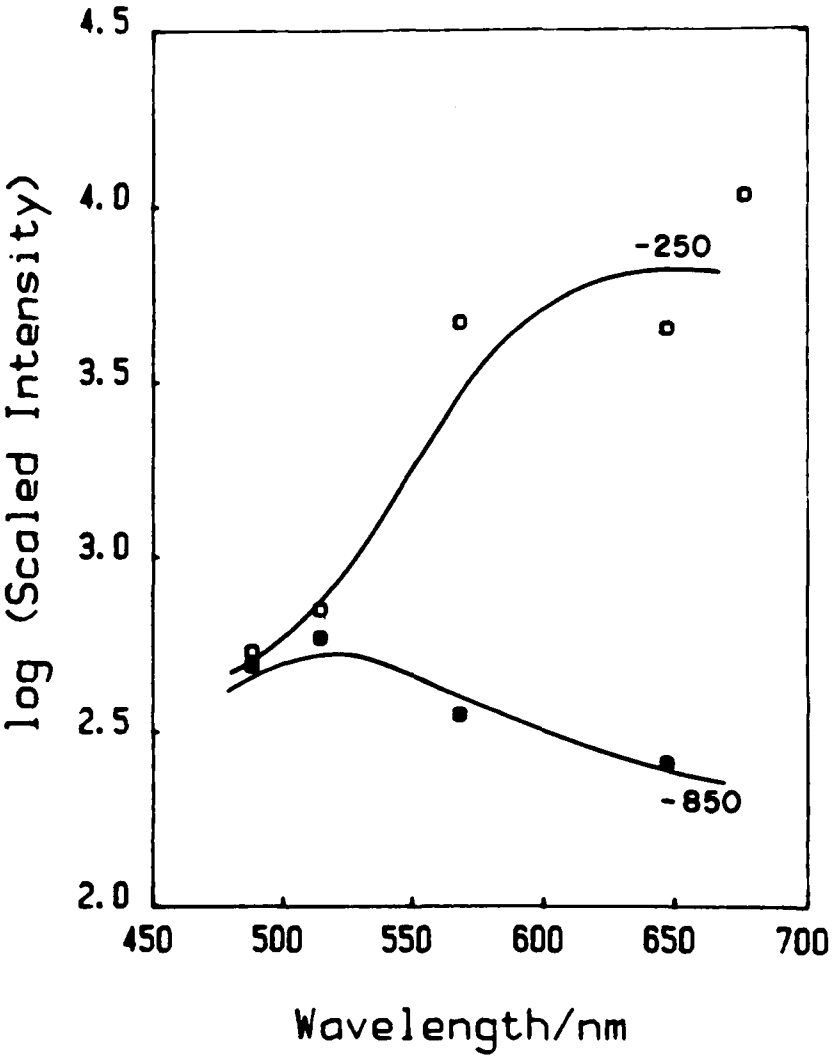

Figure 11. The shift of the excitation profile of ν_s with applied potential.

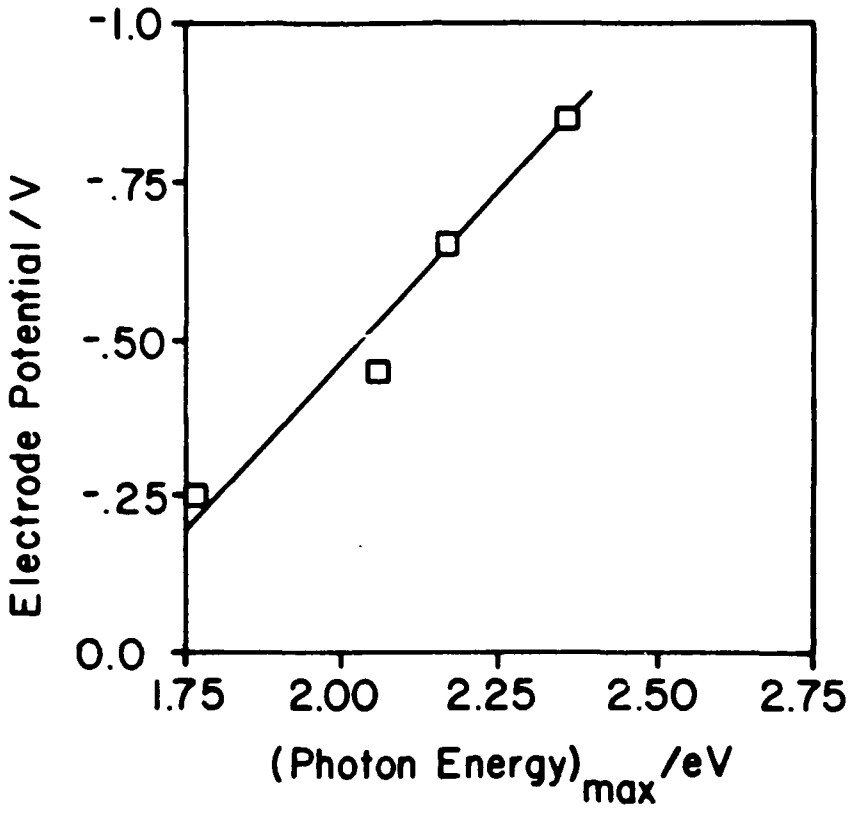

Figure 12. A plot of the electrode potential versus the photon energy at the maximum of the excitation profiles.

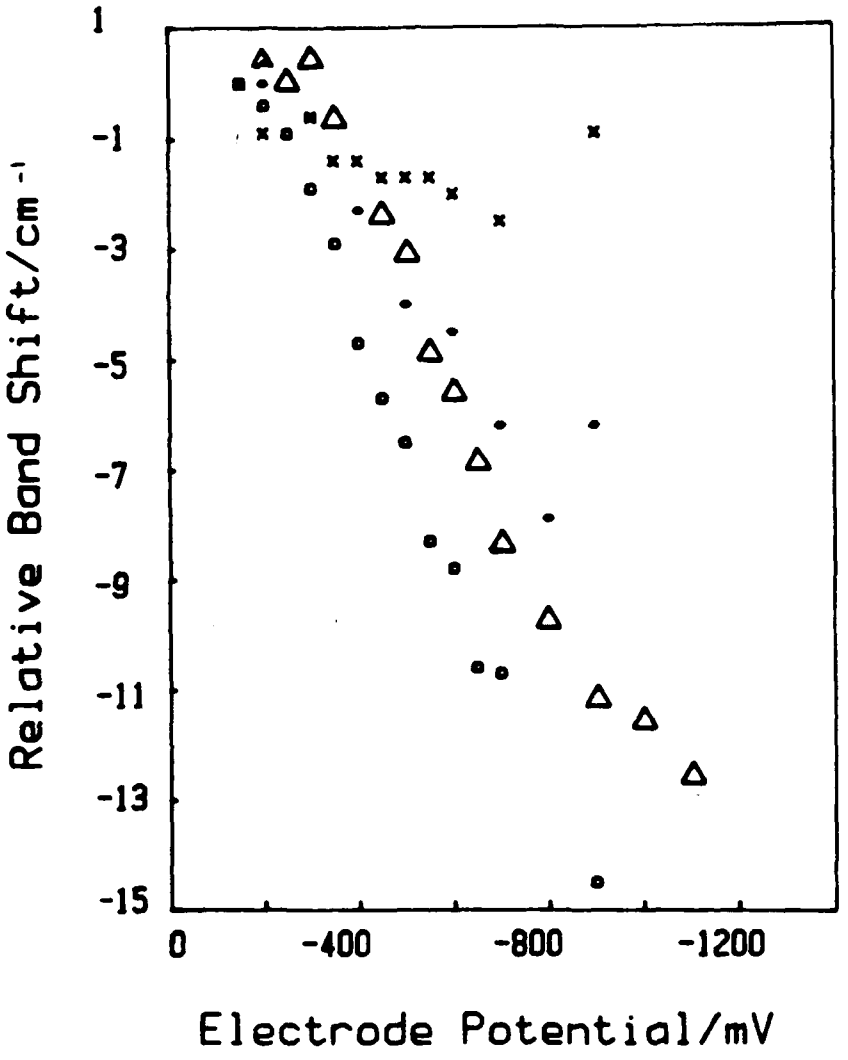

Figure 13. The relative band frequencies of the four strongest DABCO bands as a function of the electrode potential. The crosses are ν_5, the asterisks ν_6, the triangles ν_4 and the open circles ν_3.

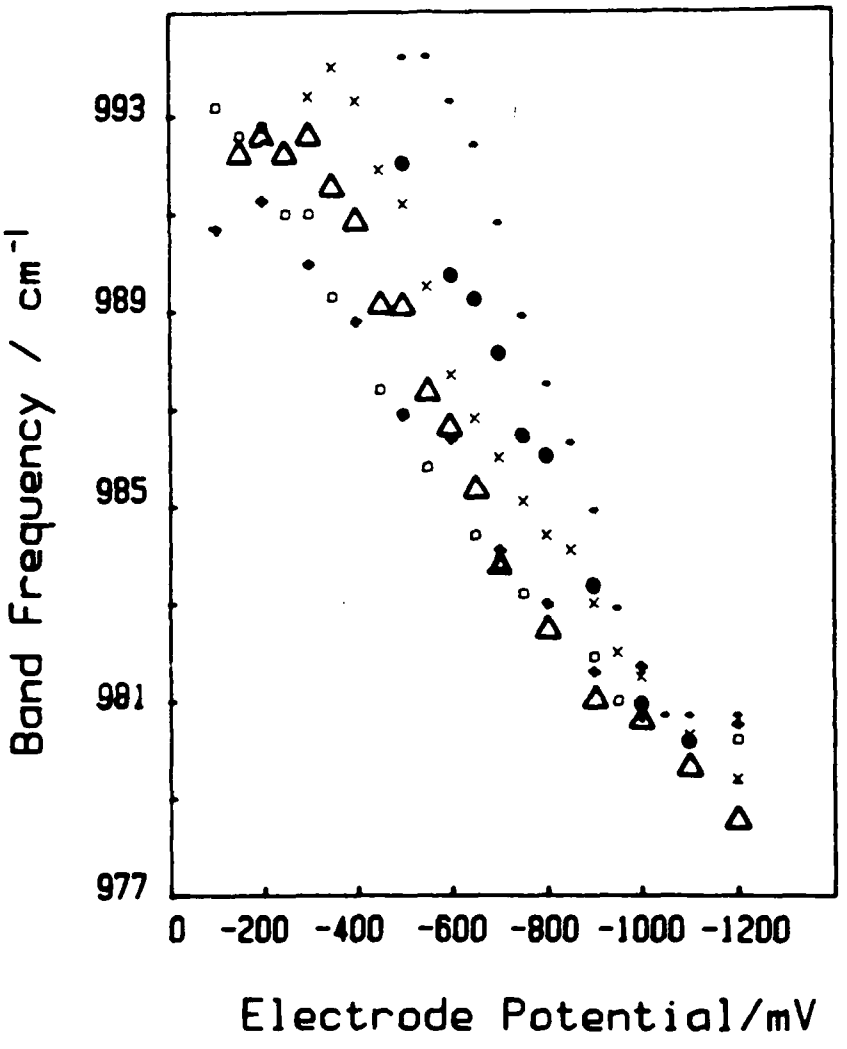

Figure 14. The variation of the frequency of ν_4 with electrode potential in different supporting electrolytes. The open circles are the perchlorate data, the plusses are the fluoride data, the triangles, crosses and filled circles are the data for 0.1, 0.5 and 1.0 M chloride, respectively, and the asterisks are the data for 0.1 M bromide.

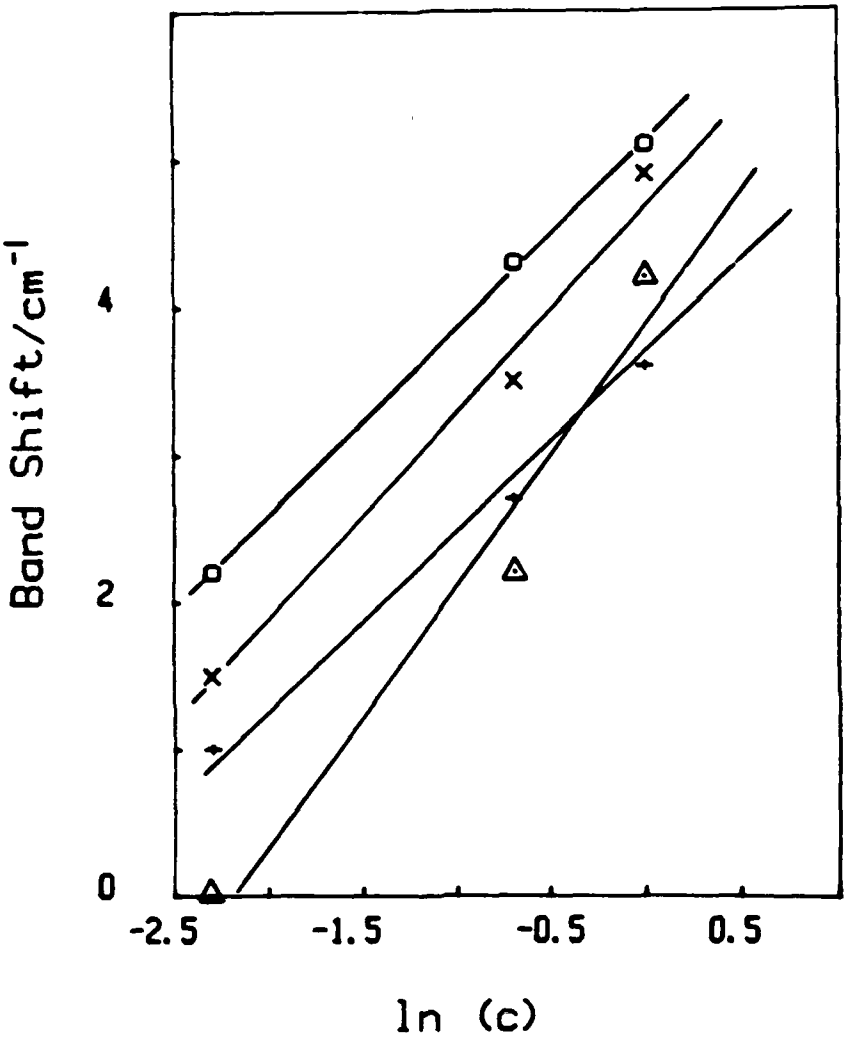

Figure 15. The change in the frequency of ν_4 versus the logarithm of the anion concentration. The open circles, crosses, pluses and triangles are the data points for -500, -550, -600 and -700 mV, respectively.

DL/1113/87/2

TECHNICAL REPORT DISTRIBUTION LIST, GEN

	No. Copies
Office of Naval Research Attn: Code 1113 800 N. Quincy Street Arlington, Virginia 22217-5000	2
Dr. Bernard Douda Naval Weapons Support Center Code 50C Crane, Indiana 47522-5050	1
Naval Civil Engineering Laboratory Attn: Dr. R. W. Drisko, Code L52 Port Hueneme, California 93401	1
Defense Technical Information Center Building 5, Cameron Station Alexandria, Virginia 22314	12 high quality
DTNSRDC Attn: Dr. H. Singerman Applied Chemistry Division Annapolis, Maryland 21401	1
Dr. William Tolles Superintendent Chemistry Division, Code 6100 Naval Research Laboratory Washington, D.C. 20375-5000	1
Dr. David Young Code 334 NORDA NSTL, Mississippi 39529	1
Naval Weapons Center Attn: Dr. Ron Atkins Chemistry Division China Lake, California 93555	1
Scientific Advisor Commandant of the Marine Corps Code RD-1 Washington, D.C. 20380	1
U.S. Army Research Office Attn: CRD-AA-IP P.O. Box 12211 Research Triangle Park, NC 27709	1
Mr. John Boyle Materials Branch Naval Ship Engineering Center Philadelphia, Pennsylvania 19112	1
Naval Ocean Systems Center Attn: Dr. S. Yamamoto Marine Sciences Division San Diego, California 91232	1